NANO LETTERS

2007
Vol. 7, No. 7
1947−1952

Plasmonic Properties of Copper Nanoparticles Fabricated by Nanosphere Lithography

George H. Chan, Jing Zhao, Erin M. Hicks, George C. Schatz,* and Richard P. Van Duyne*

Department of Chemistry, Northwestern University, 2145 Sheridan Road, Evanston, Illinois 60208-3113

Received March 19, 2007; Revised Manuscript Received May 29, 2007

ABSTRACT

The localized surface plasmon resonance (LSPR) of oxide-free Cu nanoparticles fabricated by nanosphere lithography is examined by UV–vis extinction spectroscopy and electrodynamics theory. The LSPR of the Cu nanoparticles is significantly affected by the presence of copper oxides and the removal of the oxide species yields a dramatic difference in the observed LSPR. From a comparison of the LSPR of Cu, Ag, and Au nanoparticles of similar geometry, we conclude that Cu displays an intense and narrow LSPR peak that is comparable to Ag and Au.

Copper is the most abundantly used metal in electronics applications due to its high conductivity and low cost. The development of miniaturized nanodevices that integrate electronic, photonic, chemical, and/or biological features is important for future electronic and sensing devices. The large extinction cross section and photosensitivity of noble metal nanostructures make them promising platforms as highly sensitive optical nanosensors, photonic components, and in surface-enhanced spectroscopies.[1−10] The signature optical response of interest is known as the localized surface plasmon resonance (LSPR).[11,12] The LSPR is excited when light (electromagnetic radiation) interacts with the free (conduction) electrons of a metallic nanostructure, which results in the collective excitations (oscillations) that lead to strong enhancements of the local electromagnetic fields surrounding the nanoparticles. Previous studies found that the intensity, line width, and extinction maximum wavelength of the LSPR (λ_{max}) is highly sensitive to the size, shape, interparticle spacing, dielectric environment, and dielectric properties of the nanoparticles.[13−16]

It is well-established that noble metal nanoparticles, in particular, Ag and Au, support plasmon resonances that can be tuned throughout the UV−vis−NIR region.[17,18] In addition, the plasmonic properties of Pt and Pd nanodisk arrays fabricated by the hole−mask lithography were found to exhibit LSPR's that are broader and weaker than Ag.[19] The requirement for LSPR is a large negative real and a small imaginary dielectric function, thus a number of other metals (i.e., Li, Na, Al, In, Ga, and Cu) meet this criterion and in theory should support plasmon resonances for at least part of the UV−vis−NIR region.[11,20] However, most of these metals are either unstable, difficult to work with, or prone to surface oxidation that can significantly affect the optical properties. As a result of surface oxidation, the plasmonic properties of Cu have not received much attention as compared to Ag and Au.

Copper metal is prone to surface oxidation upon exposure to ambient laboratory atmosphere at room temperature; in this case, the dominant product is Cu_2O and the minor product is CuO.[21] Various protection methods have been implemented in order to prevent the oxidation of copper. For example, copper nanoparticles have been embedded into a transparent matrix to prevent oxidation and to study their optical properties.[22,23] However, the encapsulation of the copper nanoparticles in a transparent matrix precludes the systematic study of their optical properties (i.e., lack of control over size and interparticle spacing), refractive-index sensitivities, and surface enhanced properties. An alternative approach is to fabricate nanoparticles in solution. The optical properties of colloidal copper nanoshells[24] and copper nanocrystals[25] in solution have been reported. In the case of copper nanoshells, when the plasmon resonance (dipole or quadrupole) of the Cu nanoshell overlapped with the interband transitions of Cu, a broad double-peaked plasmon resonance was observed. In the case of the copper nanocrystals (a few nm in size), the dipolar plasmon resonance was found to be dependent on the shape (triangular prisms, elongated particles, cylinders, and spheres) of the copper nanocrystals. However, the lack of homogeneity in the size

* Corresponding authors. E-mail: vanduyne@northwestern.edu (R.P.V.D.); schatz@chem.northwestern.edu (G.C.S.). Telephone: (847) 491-3516 (R.P.V.D.); (847) 491-5657 (G.C.S.). Fax: (847) 491-7713 (R.P.V.D.); (847) 491-7713 (G.C.S.).

10.1021/nl070648a CCC: $37.00
Published on Web 06/13/2007

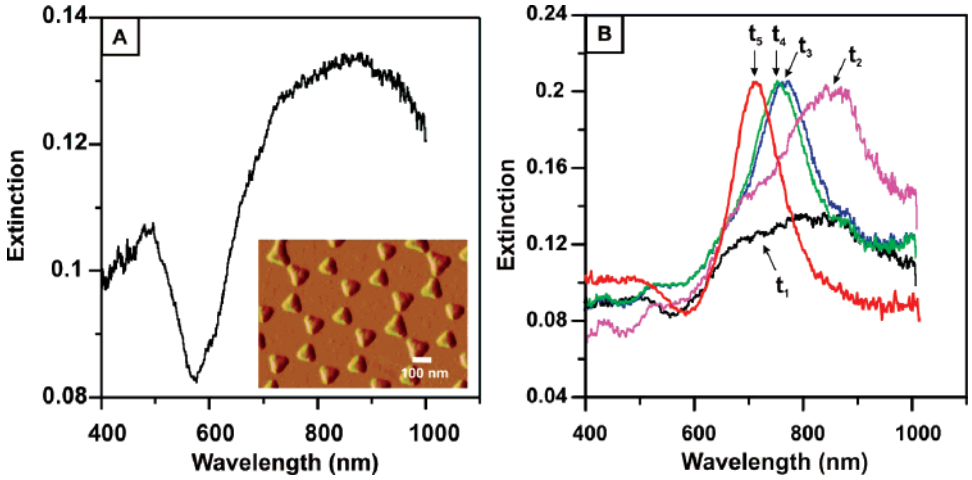

Figure 1. Extinction spectra of Cu nanoparticle arrays (D = 390 nm, d_m = 40 nm, glass substrate). (A) Extinction spectrum of an oxidized sample (inset: AFM image of the sample); (B) real-time extinction spectra tracking the change in the LSPR during oxide removal with glacial acetic acid, where t_1 = 0 s (black), t_2 = 2 s (light purple), t_3 = 10 s (blue), t_4 = 20 s (green, λ_{max} = 760 nm) in acetic acid, and t_5 = final (red, λ_{max} = 710 nm) in a N_2 environment.

and shape of the samples and the lack of control over the interparticle distances result in broadened surface plasmon resonances, which suggest that Cu metal is not an ideal plasmonic material as compared to Ag and Au.

In this work, we examine the optical properties of surface-confined Cu nanoparticles fabricated by nanosphere lithography (NSL).[26] A simple oxide removal procedure using glacial acetic acid was implemented to study the effect of Cu oxides on the LSPR of the Cu nanoparticles with UV−vis extinction spectroscopy, and the experimental results were compared with electrodynamics calculations using the discrete dipole approximation (DDA) method. We demonstrate that removal of the copper oxide species yields a dramatic difference in the observed LSPR. Through the selection of the nanosphere diameter (D) and the deposited metal thickness (d_m), the geometry and interparticle spacing of the copper nanoparticles can be controlled and the LSPR can be systematically tuned throughout the visible region in a N_2 environment. Finally, a comparison of the experimental and theoretical LSPR of Cu, Ag, and Au nanoparticles of similar size and shape is presented.

Fisher brand no. 2, 18 mm diameter glass coverslips were obtained from Fisher Scientific. Glass substrates and Si substrates were cleaned in a piranha solution (1:3 30% H_2O_2:H_2SO_4) at 80 °C for 30 min. (CAUTION: *Piranha reacts violently with organic compounds and should be handled with great care!*) Samples were allowed to cool and then rinsed repeatedly with ultrapure water (18.2 MΩ·cm Marlborough, MA). The samples were then sonicated in a (5:1:1 H_2O:NH_4OH:30% H_2O_2) solution for 1 h and then rinsed with copious amounts of ultrapure water. Polystyrene nanospheres with diameters of 280, 390, 450, 500, and 590 nm were received as a suspension in water (Interfacial Dynamics Corp., Portland, OR, or Duke Scientific, Palo Alto, CA). Copper, silver, or gold metal was deposited by electron beam (e-beam) deposition in a Kurt J. Lesker Axxis e-beam deposition system (Pittsburgh, PA) with a base pressure of 10^{-6} Torr. The mass thickness and the deposition rate (0.5 Å s^{-1}) were monitored using a Sigma Instrument 6 MHz gold-plated QCM (Fort Collins, CO). After the metal deposition, the nanosphere masks were removed by sonication in absolute ethanol (Pharmco, Brookfield, CT) for 3 min. The sample was then placed in a home-built flow cell and subsequently introduced into a N_2 environment to dry the sample. Macroscale UV−visible extinction measurements in a standard transmission geometry mode were performed using an Ocean Optics model SD2000 (Dunedin, FL) with unpolarized white light provided by a tungsten−halogen light source. The light spot diameter was approximately 1−2 mm. The extinction maximum was located by calculating the zero-crossing point of the first derivative.

Figure 1A illustrates a representative LSPR spectrum for a freshly prepared sample where D = 390 nm and d_m = 40 nm. The LSPR of the sample is very broad and the peak intensity (~0.06 extinction unit) is small. This spectral pattern was consistently observed for different samples prepared with various nanosphere diameters and nanoparticle heights. It is presumed that the broadening of the LSPR peak is from the presence of a copper oxide shell surrounding the copper metal core to form a core−shell nanoparticle. Studies on oxidized copper thin films indicate that copper oxides can be effectively removed via glacial acetic acid without attacking the underlying copper metal film because copper metal has an excellent resistance to corrosion in the presence of acetic acid.[27,28] Acetic acid reacts with copper oxides and not with copper metal to form cupric acetate by the following reactions: (1) $CuO + 2CH_3COOH \rightarrow Cu(CH_3COO)_2 + H_2O$ and (2) $Cu_2O + 4CH_3COOH \rightarrow 2Cu(CH_3COO)_2 + H_2O + H_2$. X-ray photoelectron spectroscopy (XPS) studies on the copper films indicate that no species other than metallic Cu was found when acetic acid was used as the etchant to remove copper oxides and N_2 gas was used to dry the sample.[27] Acetic acid has a low surface tension (27.8 dyn/cm), which allows for easy removal from the surface of the NSL Cu nanoparticles with N_2 gas.[29]

As described above, the extinction spectrum for a NSL Cu nanoparticle sample (D = 390 nm and d_m = 40 nm) in N_2 prior to acetic acid treatment was recorded and is shown

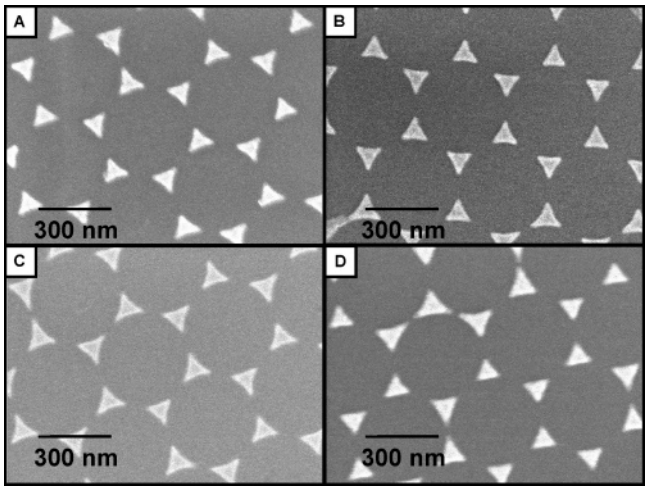

Figure 2. SEM images confirming that the structure (triangular) of the copper nanoparticles are similar before and after glacial acetic acid treatment (D = 390 nm; silicon substrate): (A) d_m = 20 nm, untreated; (B) d_m = 20 nm, acetic acid treated; (C) d_m = 40 nm, untreated; (D) d_m = 40 nm, acetic acid treated.

in Figure 1A, B (at t_1 = 0, black spectrum). Glacial acetic acid was then slowly pumped into the flow cell, and a dramatic difference in the extinction spectrum was observed. Representative LSPR spectra monitoring the change as the copper oxides were removed are shown in Figure 1B. The LSPR spectrum (green spectrum) of the copper nanoparticles in a solution of glacial acetic acid was found to stabilize at a λ_{max} of 760 nm. Following acetic acid treatment, the sample was then dried with N_2 gas and the LSPR was recorded again in an N_2 environment; the LSPR was found to stabilize at a λ_{max} of 710 nm (red peak). The total amount of time needed to completely remove the copper oxides was about 20 s. This was determined from the amount of time it took for the LSPR to stabilize in acetic acid. Stabilization of the LSPR indicates complete oxide removal on the surface of the copper nanoparticles.

The height and the structure of the copper nanoparticles were investigated with both atomic force microscope (AFM) and scanning electron microscope (SEM) prior to and upon treatment with glacial acetic acid. Tapping-mode AFM images were collected using a Digital Instruments Nanoscope IV microscope and a Nanoscope IIIA controller (Digital Instruments, Santa Barbara, CA). SEM images were collected using a Hitachi-4500 SEM at an accelerating voltage of 10 kV and an average working distance of 7 mm on samples prepared on Si substrates. The inset in Figure 1A depicts a typical AFM image of an untreated copper nanoparticle sample. The shape of the untreated copper nanoparticles is nearly triangular and the height of this particular sample is ~40 nm and is in good agreement with the measurement from the quartz crystal microbalance in the deposition system. After the sample was incubated in glacial acetic acid (less than 1 min) and allowed to dry, the heights of the copper nanoparticles were remeasured with AFM. From the AFM studies, the amount of copper oxides present on the surface of the NSL copper nanoparticles after 3−8 min exposure to ambient laboratory conditions at room temperature is most likely very thin. It is estimated to be approximately less than 1 nm. Studies of room-temperature oxide growth on spherical copper nanoparticles (diameter = 100 and 140 nm) indicate that initial oxide growth is also very slow (~0.031 nm/day) and that growth of copper oxides is continuous with the thickness of the copper oxides increasing with time.[21] SEM images of two different NSL fabricated Cu samples (where D = 390 nm and d_m = 20 and 40 nm) on a Si substrate before and after acetic acid treatment are illustrated in Figure 2. The structure of the copper nanoparticles is triangular both before and after glacial acetic acid treatment, in accordance with AFM studies.

It is clear from the AFM and SEM studies that the removal of the copper oxides with glacial acetic acid does not significantly affect the shape and the height of the copper nanoparticles. Moreover, the LSPR peak of the NSL Cu nanoparticles (Figure 1B) was narrower and more intense after the copper oxides were removed. To further examine the LSPR properties, the oxide-removed particles were fabricated with varying out-of-plane heights and in-plane widths, and the observed spectra were compared with the results of classical electrodynamics calculations based on the DDA method.[30,31] In all the calculations, the particles are assumed to be truncated tetrahedra, with dielectric constants

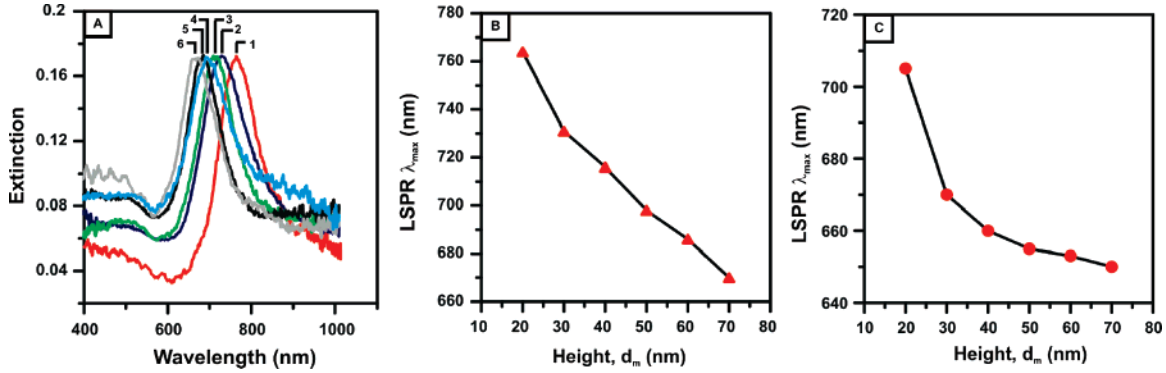

Figure 3. (A) Extinction spectra of the Cu nanoparticle arrays after acetic acid treatment (D = 390 nm, d_m = 20−70 nm). All spectra were collected in a N_2 environment. Spectrum 1 (red), d_m = 20 nm, λ_{max} = 764 nm; spectrum 2 (dark blue), d_m = 30 nm, λ_{max} = 730 nm; spectrum 3 (green), d_m = 40 nm, λ_{max} = 713 nm; spectrum 4 (light blue), d_m = 50 nm, λ_{max} = 698 nm; spectrum 5 (black), d_m = 60 nm, λ_{max} = 685 nm; and spectrum 6 (light gray), d_m = 70 nm, λ_{max} = 670 nm. LSPR $\lambda_{max.}$ vs nanoparticle height (d_m) shown for the experimental (B) and calculated (C) results.

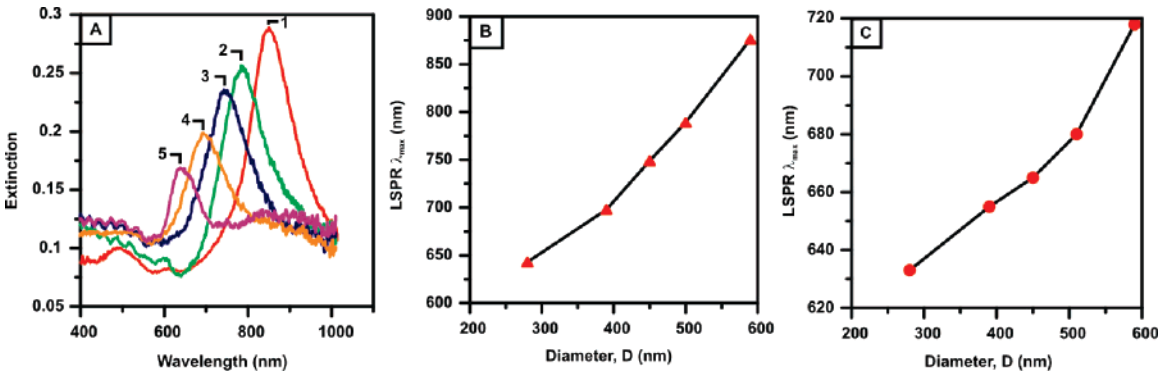

Figure 4. (A) Extinction spectra of Cu nanoparticle arrays with varying widths after acetic acid treatment (D = 280−590 nm; d_m = 50 nm). All spectra were collected in a N_2 environment. Spectrum 1 (red), D = 590 nm, λ_{max} = 876 nm; spectrum 2 (green), D = 500 nm, λ_{max} = 789 nm; spectrum 3 (blue), D = 450 nm, λ_{max} = 750 nm; spectrum 4 (orange), D = 390 nm, λ_{max} = 698 nm, and spectrum 5 (purple), D = 280 nm, and λ_{max} = 643 nm. LSPR λ_{max} vs diameter (D) shown for the experimental (B) and calculated (C) results.

taken from Lynch and Hunter.[32] The effect of the glass on the LSPR was treated using the effective medium theory.[33] The particles are assumed to be embedded in a homogeneous medium where the dielectric constant is a weighted average of that for the glass and that for N_2, with the weighting determined by the relative fractions of the particles that are exposed to each medium.

The measured extinction spectra of NSL copper nanoparticle arrays with heights varying from d_m = 20−70 nm with a fixed nanosphere diameter (D = 390 nm) are illustrated in Figure 3A. The intensity of the LSPR peak is ~0.1 extinction unit. As the height of the nanoparticle increases from 20 to 70 nm, a blue-shift in the LSPR λ_{max} is observed. A blue-shift in the LSPR λ_{max} with an increase in the nanoparticle height was also observed for Ag and Au NSL nanoparticle arrays.[34−36] The comparison of the experimental and calculated LSPR λ_{max} as a function of nanoparticle height is shown in parts B and C of Figure 3, respectively. The experimental position of the LSPR λ_{max} agrees at least qualitatively with the predictions of theory; as the height of the nanoparticle decreases, the LSPR λ_{max} red-shifts. For a given height change, this shift is larger for the shorter nanoparticles than is for the taller nanoparticles. For example, the experimental shift in λ_{max} is 15 nm for a change in nanoparticle height from 60 to 70 nm, whereas the shift is 27 nm for a change of the nanoparticle height from 30 to 40 nm. This behavior is consistent with theory, and in fact, earlier theoretical studies concerning this were reported for Au triangular prisms.[37]

The extinction spectra of copper nanoparticles with fixed height, d_m = 50 nm, and varying nanosphere diameters (D = 280, 390, 450, 500, and 590 nm) are illustrated in Figure 4A. The intensity of the LSPR peak increases as the nanosphere diameter becomes larger. The fwhm (full width at half-maximum) of the LSPR's range from 0.22 to 0.28 eV. As the LSPR approaches the interband transitions (E = 2.1 eV corresponding to a wavelength of 590 nm) of Cu, a significant decrease in the intensity of the LSPR is observed, which differs from that of Ag. Comparisons of experimental and calculated LSPR λ_{max} as a function of nanosphere diameter (parts B and C of Figure 4, respectively) show

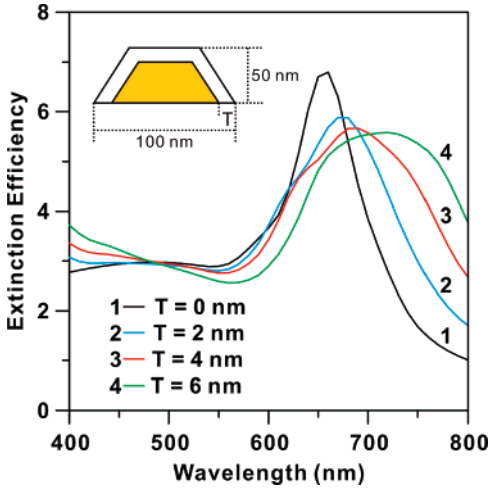

Figure 5. DDA simulations of the effect of oxidation of copper (Cu_2O) on a NSL Cu nanoparticle at room temperature. Calculations were performed for a nanoparticle with a Cu core surrounded by a Cu_2O shell. The inset shows a side view of the core−shell nanoparticle. The total height and width of the nanoparticle was fixed at 50 and 100 nm, respectively. The thicknesses (T) of the Cu_2O shell were varied from 0 to 6 nm.

qualitative agreement, but the overall shift is smaller in the calculations. This discrepancy is likely due to differences between the fabricated and calculated particle shape, as the truncated tetrahedron model is only a rough approximation to what is fabricated using NSL. In addition, the effective medium model for substrate effects tends to underestimate the observed substrate effect for particles with high aspect ratios.

Theoretical simulation of the effect of Cu_2O on the extinction spectra of a copper nanoparticle with a fixed height of 50 nm and a perpendicular bisector of 100 nm is illustrated in Figure 5. The dominant oxidation product of copper metal at room temperature is Cu_2O. The dielectric functions of Cu_2O, CuO, and $CuO_{0.67}$ are very similar, and the dielectric function of Cu_2O was used in the DDA simulations.[38,39] The total height and width of the Cu_2O and Cu metal were fixed while the thickness of the Cu_2O shell was varied from 0 to 6 nm (Figure 5). The nanoparticle was constructed from simple core−shell geometry, i.e., a copper core surrounded

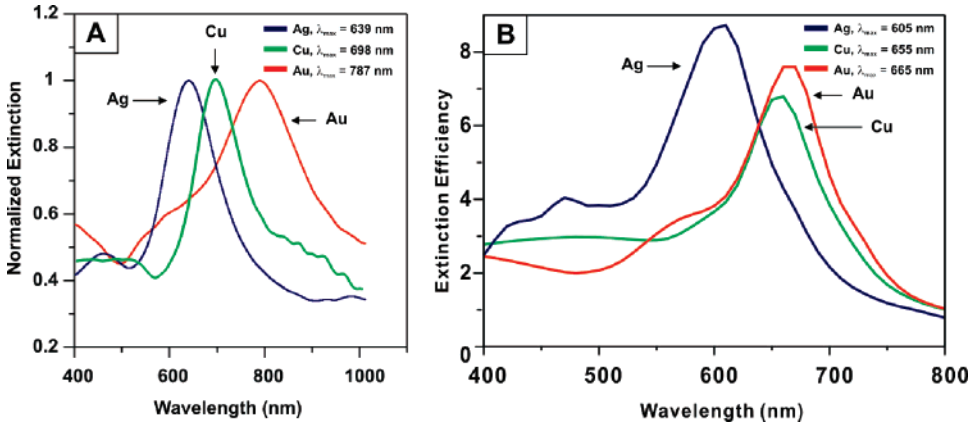

Figure 6. Comparison of the LSPR of Cu, Ag, and Au for (A) experiment and (B) theoretical calculations for a similar size and shape (D = 390 nm; d_m = 50 nm; glass substrate; N_2 environment).

with a shell of Cu_2O. Spectrum 1 (black) depicts the LSPR spectrum for a bare copper metal nanoparticle. The LSPR peak has a well-defined shape and shows a broad shoulder below 590 nm originating from the interband transitions of copper. In spectrum 2 (blue), the LSPR red-shifts and the intensity decreases when a 2 nm layer of Cu is replaced by Cu_2O. As the thickness of Cu_2O increases, the LSPR peak red-shifts and the intensity of the peak decrease until finally a broad peak is observed. These results mimic what is seen in Figure 1 quite accurately. Although the thickness of the copper oxide layer needed to match the experimental results is overestimated in the DDA simulations, the calculations confirm that the presence of copper oxides can greatly affect the LSPR. This behavior is similar to observations for oxidized copper granules (5.5 ± 0.5 nm) consisting of a copper core and an oxide shell.[40]

The removal of copper oxides allows for the first experimental comparison of the LSPR of Cu, Ag, and Au nanoparticles of similar size and shape. Figure 6A illustrates the normalized extinction spectra of Cu, Ag, and Au nanoparticle arrays fabricated by NSL where D = 390 nm and d_m = 50 nm. The LSPR λ_{max} of Cu, Ag, and Au is 698, 639, and 787 nm, respectively. The LSPR λ_{max} of Cu and Au are at longer wavelengths than for Ag nanoparticle arrays of similar geometry. The interband transitions of Cu and Au do not significantly affect the LSPR. From the comparison of the LSPR of Cu, Ag, and Au, we conclude that Cu displays an intense and narrow LSPR peak that is comparable to Ag and Au when the LSPR λ_{max} > ~650 nm. The Cu LSPR line width and line shape are surprisingly more similar to Ag than to Au. Moreover, the results from experiment agree with the predicted trends from the DDA calculations where the LSPR λ_{max} of Au > Cu > Ag for nanoparticles of the same geometry (Figure 6B). The discrepancy of the Au LSPR λ_{max} between experiment and theory can be attributed to the difference in the dewetting properties of the noble metals on glass substrates and from differences in their surface melting temperatures.[26,35] In particular, gold particles can wet the surface to produce a tiny "apron" of metal around the particle, resulting in a red-shifting of the plasmon resonance relative to what is modeled by the DDA calculation. Such effects were previously studied for annealed silver particles and can easily produce red-shifts similar to what we find.[41]

In conclusion, the plasmonic properties of copper nanoparticles fabricated by NSL have been examined by UV−vis extinction spectroscopy for the first time. It was found that the optical properties of the copper nanoparticle arrays are significantly affected by the presence of copper oxides. Removal of the copper oxides with glacial acetic acid yields a dramatic difference in the observed LSPR. In contrast to previous studies on copper nanoparticles, an intense and narrow Cu LSPR peak was observed for the NSL Cu nanoparticle arrays. Systematic studies of LSPR λ_{max} as a function of particle aspect ratio were found to agree with the trends predicted from theoretical calculations. AFM and SEM studies indicate that the amount of copper oxides on the surface of the NSL Cu nanoparticles is very small and the shape of the nanoparticles is preserved upon removal of the copper oxides. The first comparison of the LSPR of Cu, Ag, and Au nanoparticles with the same geometry was presented. These results indicate that Cu may potentially be used to replace the more expensive metals of Ag and Au for certain applications. Current work is underway to explore the refractive-index sensitivity and surface enhanced Raman spectroscopy (SERS)[42] activity of Cu as compared to Ag and Au NSL nanoparticle arrays. The versatile oxide removal procedure presented here can be easily applied to other lithographic techniques (e.g., e-beam lithography) to study the plasmonic properties of Cu nanoparticles with geometries that differ from those produced by NSL. In addition, this work opens the way to study catalytic properties[43] and copper oxide growth[44,45] in a controlled environment utilizing the optical properties of NSL copper nanoparticle arrays.

Acknowledgment. This work was supported by the National Science Foundation (EEC-0118025, CHE-0414554, BES-0507036), the Air Force Office of Scientific Research MURI program (F49620-02-1-0381), DTRA JSTO program (FA9550-06-1-0558), and the MRSEC program of the National Science Foundation (DMR-0520513) at the Materials Research Center of Northwestern University.

References

(1) Nie, S. M.; Emory, S. R. *Science* **1997**, *275*, 1102−1106.
(2) Dieringer, J. A.; McFarland, A. D.; Shah, N. C.; Stuart, D. A.; Whitney, A. V.; Yonzon, C. R.; Young, M. A.; Zhang, X.; Van Duyne, R. P. *Faraday Discuss.* **2006**, *132*, 9−26.
(3) Chen, K.; Durak, C.; Heflin, J. R.; Robinson, H. D. *Nano Lett.* **2007**, *7*, 254−258.
(4) Zhao, J.; Das, A.; Zhang, X.; Schatz, G. C.; Sligar, S. G.; Van Duyne, R. P. *J. Am. Chem. Soc.* **2006**, *128*, 11004−11005.
(5) Yonzon, C. R.; Jeoung, E.; Zou, S.; Schatz, G. C.; Mrksich, M.; Van Duyne, R. P. *J. Am. Chem. Soc.* **2004**, *126*, 12669−12676.
(6) Moran, A. M.; Sung, J.; Hicks, E. M.; Van Duyne, R. P.; Spears, K. G. *J. Phys. Chem. B* **2005**, *109*, 4501−4506.
(7) Haes, A. J.; Chang, L.; Klein, W. L.; Van Duyne, R. P. *J. Am. Chem. Soc.* **2005**, *127*, 2264−2271.
(8) Haes, A. J.; Hall, W. P.; Chang, L.; Klein, W. L.; Van Duyne, R. P. *Nano Lett.* **2004**, *4*, 1029−1034.
(9) Jiang, J.; Bosnick, K.; Maillard, M.; Brus, L. *J. Phys. Chem. B* **2003**, *107*, 9964−9972.
(10) Li, Y.; Lee, H. J.; Corn, R. M. *Anal. Chem.* **2007**, *79*, 1082−1088.
(11) Bohren, C. F.; Huffman, D. R. *Absorption and Scattering of Light by Small Particles*; John Wiley & Sons: New York, 1983.
(12) Kreibig, U.; Vollmer, M. *Optical Properties of Metal Clusters*; Springer-Verlag: Heidelberg, 1995; Vol. 25.
(13) Haynes, C. L.; Van Duyne, R. P. *J. Phys. Chem. B* **2001**, *105*, 5599−5611.
(14) Sherry, L. J.; Jin, R.; Mirkin, C. A.; Schatz, G. C.; Van Duyne, R. P. *Nano Lett.* **2006**, *6*, 2060−2065.
(15) Sherry, L. J.; Chang, S. H.; Schatz, G. C.; Van Duyne, R. P.; Wiley, B. J.; Xia, Y. *Nano Lett.* **2005**, *5*, 2034−2038.
(16) Huang, W. Y.; Qian, W.; El-Sayed, M. A. *Nano Lett.* **2004**, *4*, 1741−1747.
(17) Murray, W. A.; Suckling, J. R.; Barnes, W. L. *Nano Lett.* **2006**, *6*, 1772−1777.
(18) Nehl, C. L.; Liao, H. W.; Hafner, J. H. *Nano Lett.* **2006**, *6*, 683−688.
(19) Langhammer, C.; Yuan, Z.; Zoric, I.; Kasemo, B. *Nano Lett.* **2006**, *6*, 833−838.
(20) Zeman, E. J.; Schatz, G. C. *J. Phys. Chem.* **1987**, *91*, 634−643.
(21) Kim, J. H.; Ehrman, S. H.; Germer, T. A. *Appl. Phys. Lett.* **2004**, *84*, 1278−1280.
(22) Yeshchenko, O. A.; Dmytruk, I. M.; Alexeenko, A. A.; Dmytruk, A. M. *Phys. Rev. B* **2007**, *75*, 085434-1−085434-6.
(23) Zong, R. L.; Zhou, J.; Li, B.; Fu, M.; Shi, S. K.; Li, L. T. *J. Chem. Phys.* **2005**, *123*, 094710-1−094710-5.
(24) Wang, H.; Tam, F.; Grady, N. K.; Halas, N. J. *J. Phys. Chem. B* **2005**, *109*, 18218−18222.
(25) Salzemann, C.; Brioude, A.; Pileni, M. P. *J. Phys. Chem. B* **2006**, *110*, 7208−7212.
(26) Hulteen, J. C.; Treichel, D. A.; Smith, M. T.; Duval, M. L.; Jensen, T. R.; Van Duyne, R. P. *J. Phys. Chem. B* **1999**, *103*, 3854−3863.
(27) Chavez, K. L.; Hess, D. W. *J. Electrochem. Soc.* **2001**, *148*, G640−G643.
(28) *Metals Handbook*, 2nd ed.; American Society for Metals International: Materials Park, OH, 1998; p 554.
(29) *CRC Handbook of Chemistry and Physics*, 69th ed.; CRC Press: Boca Raton, FL, 1989.
(30) Draine, B. T.; Flatau, P. J. *J. Opt. Soc. Am. A* **1994**, *11*, 1491−1499.
(31) Jensen, T.; Kelly, L.; Lazarides, A.; Schatz, G. C. *J. Cluster Sci.* **1999**, *10*, 295−317.
(32) Lynch, D. W.; Hunter, W. R. In *Handbook of Optical Constants of Solids*; Palik, E. D., Ed. Academic Press: New York, 1985; pp 350−356.
(33) Malinsky, M. D.; Kelly, K. L.; Schatz, G. C.; Van Duyne, R. P. *J. Phys. Chem. B* **2001**, *105*, 2343−2350.
(34) Jensen, T. R.; Schatz, G. C.; Van Duyne, R. P. *J. Phys. Chem. B* **1999**, *103*, 2394−2401.
(35) Huang, W. Y.; Qian, W.; El-Sayed, M. A. *J. Phys. Chem. B* **2005**, *109*, 18881−18888.
(36) Haes, A. J.; Zou, S. L.; Schatz, G. C.; Van Duyne, R. P. *J. Phys. Chem. B* **2004**, *108*, 6961−6968.
(37) Shuford, K. L.; Ratner, M. A.; Schatz, G. C. *J. Chem. Phys.* **2005**, *123*, 114713-1−114713-8.
(38) Derin, H.; Kantarli, K. *Appl. Phys. A* **2002**, *75*, 391−395.
(39) Wieder, H.; Czanderna, A. W. *J. Phys. Chem.* **1962**, *66*, 816−821.
(40) Khairullina, A. Y.; Ol'shanskaya, T. V.; Babenko, V. A.; Kozhevin, V. M.; Yavsin, D. A.; Gurevich, S. A. *Opt. Spectrosc.* **2005**, *98*, 96−101.
(41) Whitney, A. V.; Elam, J. W.; Zou, S.; Zinovev, A. V.; Stair, P. C.; Schatz, G. C.; Van Duyne, R. P. *J. Phys. Chem. B* **2005**, *109*, 20522−20528.
(42) Schatz, G. C.; Van Duyne, R. P. *Electromagnetic Mechanism of Surface-Enhanced Spectroscopy*; Wiley: New York, 2002; pp 759−774.
(43) Kidwai, M.; Bansal, V.; Saxena, A.; Aerry, S.; Mozumdar, S. *Tetrahedron Lett.* **2006**, *47*, 8049−8053.
(44) Yanase, A.; Matsui, H.; Tanaka, K.; Komiyama, H. *Surf. Sci.* **1989**, *219*, L601−L606.
(45) Yanase, A.; Komiyama, H. *Surf. Sci.* **1991**, *248*, 11−19.

NL070648A